A study of the open circuit voltage characterization technique and hysteresis assessment of lithium-ion cells

Anup Barai*, W.D. Widanalage, James Marco, Andrew McGordon and Paul Jennings
WMG, University of Warwick, Coventry, CV4 7AL, United Kingdom

*Corresponding author: Anup Barai
WMG, The University of Warwick
Coventry, CV4 7AL, UK
E-mail: a.barai@warwick.ac.uk
Tel: +44 (0) 24 76575928
Fax: +44 (0) 24 7652 4307

Keywords
Lithium-ion battery, OCV, Hysteresis, testing, SoC estimation

Abstract

Among lithium-ion battery applications, the relationship between state of charge (SoC) and open circuit voltage (OCV) is used for battery management system operation. The path dependence of OCV is a distinctive characteristic of lithium-ion batteries which is termed as OCV hysteresis. Accurate estimation of OCV hysteresis is essential for correct SoC identification. OCV hysteresis test procedures used previously do not consider the coupling of variables that show an apparent increase in hysteresis. To study true OCV hysteresis, this paper proposes a new test methodology. Using the proposed methodology, OCV hysteresis has been quantified for different lithium-ion cells. The test results show that a battery's OCV is directly related to the discharge capacity. Measured battery capacity can vary up to 5.0% depending on the test procedure and cell chemistry. The maximum hysteresis was found in a $LiFePO_4$ (LFP) cell (38mV) and lowest in the LTO cell (16mV). A dynamic hysteresis model is used to show how better prediction accuracy can be achieved when hysteresis voltage is a function of SoC instead of assuming as a constant. The results highlight the importance of the testing procedure for OCV characterisation and that hysteresis is present in other Li-ion batteries in addition to LFP.

Abbreviations and notations

BEV	Battery Electric Vehicle
BMS	Battery Management System
CC-CV	Constant current constant voltage
DoD	Depth-of-discharge
EV	Electric Vehicle
ECM	Equivalent Circuit Model
HEV	Hybrid Electric Vehicle
LFP	Lithium Iron Phosphate
LTO	Lithium Titanate
NCM	Nickel Cobalt Manganese Oxide
OCV	Open Circuit Voltage
ODE	Ordinary Differential Equation
PHEV	Plug-in Hybrid Electric Vehicle
RV	Rest Voltage
RV_c	Charge Rest Voltage
RV_d	Discharge Rest Voltage
$(\overline{RV})$	Average rest voltage between charge and discharge
SoC	State-of-charge
z(t)	SoC at time t
w(t)	DoD at time t
Q_c (t)	Capacity during charge
Q_d (t)	Capacity during discharge
Q_r (t)	Cell remaining capacity
Q_e (t)	Extracted capacity from cell
Q_(e,max)	Maximum extracted cell capacity in Ampere-seconds

1. Introduction

Introduction of lithium-ion batteries to electric vehicles (EV), including hybrid electric vehicles (HEV), plug-in hybrid electric vehicles (PHEV), battery electric vehicles (BEV), is enabled by their high energy and power capability, long cycle life and a low purchase price [1-4]. Electrical equivalent circuit models (ECM) are commonly used to evaluate electrical performance (e.g. current, voltage, power, energy) of the battery in real world operating conditions. ECMs have a wide range of applications, varying from on-board State-of-charge (SoC) estimation [5-7] to long-term ageing estimation [8-10]. A substantial amount of research has been done on equivalent circuit modelling of the lithium-ion battery [5, 6, 11-14]. ECMs of the simplest form [11] to very complex form [12] have been proposed which represent the electrical and electrochemical behaviour of the cell.

A commonly used structure of ECM is shown in Figure 1. The values of resistances and capacitances in ECM can be determined using different techniques such as Electrochemical Impedance Spectroscopy (EIS) and pulse power test etc. [10]. These techniques are well understood and general relationships of these circuit parameters exists for different real world operating conditions like varying temperature [5, 10, 15-19] and SoC [5, 6, 10].

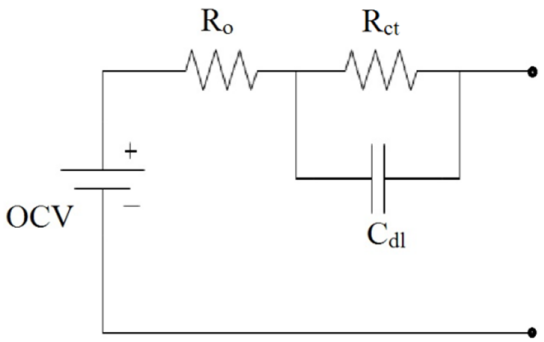

Figure 1: An equivalent circuit model showing open circuit voltage (OCV), ohmic resistance R_o, charge transfer resistance R_{ct} and double layer capacitance C_{dl}.

Open circuit voltage (OCV) is present in all forms of ECMs. The OCV is the battery thermodynamic equilibrium potential when not under a current load. The OCV as a function of SoC is an important characteristic for ECMs. It acts as an ideal but variable (e.g. with SoC) voltage source in the model to which over-potential is added by the remaining resistor and capacitor elements of the ECM.

Conversely, the SoC of a cell, which is crucial for a vehicle Battery Management System (BMS), can be determined if the cell's OCV is known. This however assumes a one-to-one relation between OCV and SoC allowing the SoC to be known via the OCV. If, however, hysteresis is present, the cell OCV during charge is different from discharge at the same SoC. The presence of any hysteresis therefore implies that knowledge of the cell open circuit potential alone is insufficient to determine the SoC without also knowing the charge-discharge history of the cell. In recent literature, the importance of hysteresis in SoC estimation using ECM has been shown [20].

OCV hysteresis can have significant influence on SoC estimation accuracy [21, 22]. An inaccuracy in SoC will be reflected as inaccurate range estimation, leading to decrease of user satisfaction/trust; which in turn is a potential business risk to the OEMs. On the other hand, the inaccuracy in SoC can lead to change of operating SoC window of EV's battery packs. To maintain minimum available power assist and regenerative capability, HEV battery packs operate within a SoC window, avoiding high and low SoC [23]. A SoC window is also used for other types of EVs to extend battery life and avoid safety failures due to overcharge and overdischarge [23, 24]. An inaccurate measurement of SoC can change the operating SoC window which will be reflected as short term (e.g. regenerative power capability) and long term performance drop (e.g decrease of expected battery life). Therefore, it is important that the ECM used by BMS should incorporate any cell hysteresis accurately.

The first step toward accurate assessment of hysteresis is the accurate assessment of OCV. As the OCV-SoC relation is typically determined empirically it is important that the experiment and subsequent calibration are performed with care. The OCV cannot be used to establish the SoC. When investigating the level of hysteresis, the SoC is determined via Coulomb counting for which an initial SoC is required. An incorrect initial SoC value can offset the charge and discharge OCV-SoC curves and incorrectly indicate that hysteresis is present.

Cells with lithium iron phosphate electrodes or nickel hydroxide electrodes are known to have stable hysteresis [20, 25, 26]. However, existing battery test standards [27-29] do not include a test procedure for OCV measurement and the identification of OCV hysteresis. Therefore, different methodologies (i.e. low current charge/discharge, incremental charge/discharge) have been used by researchers to measure OCV and OCV hysteresis [20, 22, 26, 30-35]. However, these papers too, did not provide a robust and consistent

methodology to assess OCV and OCV hysteresis. Therefore, an erroneous assessment of OCV and OCV hysteresis could be present historically, and will be discussed in detail in section 2 of this paper.

In this study the authors investigate the influence of step size on OCV measurements to establish an ideal testing protocol. This testing protocol will be used to identify OCV and OCV hysteresis of different chemistry lithium-ion cells. Lastly, the hysteresis data will be incorporated into a hysteresis transition model, to provide an example of how a better estimation of SoC can be achieved when accurate hysteresis data is used. In Section 2, a review of the origin of OCV hysteresis, previously used test procedures, issues with these procedures, and hysteresis modelling methods are introduced with reference to the relevant published work. Subsequently, the experimental method used as part of this research is shown in Section 3. In section 4, results, analysis of the results and their implications to the model are presented. Finally, the key findings are summarised in Section 5.

2. Background

2.1. Origin of hysteresis: a thermodynamic explanation

Hysteresis in a battery corresponds to the existence of several possible thermodynamic equilibrium potentials at the same SoC of the cell. Positive electrodes with lithium iron phosphate as the active material are known to exhibit a hysteretic phenomenon [30, 34]. Srinivasan and Newman [26] provided an explanation for hysteresis based on the existence of a lithium rich and lithium deficient phase within an active particle. They termed the explanation as the *path dependent shrinking core model*, whereby during discharge a shrinking particle core of Li_yFePO_4 and a growing outer crust of $Li_{(1-x)}FePO_4$ occurs, while during charge a shrinking core of $Li_{(1-x)}FePO_4$ and a growing crust of Li_yFePO4 occurs (considering mole fractions x and y are close to zero). The corresponding chemical potential of the particle, and therefore open circuit potential, can be different at the same SoC depending on this two phase particle composition. Moreover, intercalation of lithium into graphite anode is a complex process [36], which could be path dependent and contribute to hysteresis further.

More recent work in explaining hysteresis has extended the single particle two phase transition of $LiFePO_4$. Dreyer *et al.* [30] argued that if the active material particle has a non-monotonic chemical potential with regards to its lithium mole fraction and in the presence of many such particles in the positive electrode, the chemical potential of the electrode will be different at the same SoC depending of the path taken to reach the particular SoC. In comparison to the path dependent shrinking core model a notable revision is the interconnectedness of many particles with a non-monotonic chemical potential function. While in the former explanation a particle is assumed to be stable when it has reached its inhomogeneous two phase state (regions of low and high lithium mole fraction within the particle); in the latter the particle reaches a homogeneous stable state by distributing the lithium ions to neighbouring particles and decreasing its chemical potential during charge; similarly an inhomogeneous particle will admit lithium ions from neighbouring particles during discharge. This interchange of ions occurs when the mole fraction of an inhomogeneous particle reaches its maximum or minimum chemical potential (non-monotonic potential function) leading to different overall chemical potential, and therefore open-circuit potential, of the electrode depending if it is charging or discharging. By generalising this to other chemistries it is expected that hysteresis might be present. However, this had received little attention in the literature.

Active material particles with a non-monotonic chemical potential are expected in many intercalation battery systems and not only restricted to lithium iron phosphate electrodes. Bruce *et al.* [37] suggested hysteresis in $LiMnO_2$ cathode material, which could arise from the need to move phase boundaries between compositionally distinct regions as lithium ions are inserted and removed from the host structure. However this analysis is based on the hysteresis of load curves (charge-discharge voltage under ~C/10 current), which is not a true representation of OCV hysteresis discussed in this paper. When a cell is charged it is expected to have higher voltage than OCV, and lower during discharge (due to the voltage drop at R_o, R_{ct} and C_{dl} of Figure 1). Therefore, there is always expected to be hysteresis in load curves, even if there is no OCV hysteresis. As such, a certain magnitude of hysteresis is also expected to be present in other insertion electrochemical systems i.e. NMC, LTO. This is investigated in the subsequent sections of this paper.

2.2. Rest voltage vs capacity vs SoC test techniques

A possible approach to estimate a cell's open circuit voltage is to discharge and charge the cell with a low current (usually C/25), and average the measured charge and discharge voltages [37-40]. A low current is used to minimise any diffusion limitations. However, even with a low discharge/charge current (as used by [37-40]) the cell will experience kinetic contributions when it is nearly discharged or fully charged leading to a high voltage drop [26, 35]. As such the measured voltage can then no longer be assumed as the cell's OCV.

An alternative method is to discharge/charge the cell incrementally (e.g. 4 %, 10 %, 25 % SoC intervals) followed by a rest period to allow the cell dynamics to relax and reach equilibrium [40]. For this instance C-rate used (e.g. 1C) will not be an issue, since OCV is recorded after the rest period. The voltage recorded from this method, also known as the incremental OCV method, is a better estimate of the cell's OCV since the electrode kinetics are allowed to reach equilibrium before a measurement is taken. The relaxation time depends on the SoC and SoC increment, for example in [35], 6 minutes, 24 minutes and 2 hour rest intervals are used for SoC increments of 0.5 %, 1 % and 5 % respectively. In this paper the incremental OCV method is used with a maximum rest period of 4 hours to estimate the cell OCV. Even after a rest period of 4 hours the cell voltage may not have reached a thermodynamic equilibrium; however, it has been shown previously that depending on the cell, after 2 to 4 hours the electrochemical changes within the cell are negligible [40, 41]. Therefore, the measured voltage is still an approximation of the OCV and will be referred to as the cell *Rest Voltage* (RV).

The RV can either be measured while the battery is incrementally charged (RV_c) from a fully discharged state or incrementally discharged (RV_d) from a fully charged state. The RVs can then be associated with the corresponding charge (Q_c) or discharge (Q_c) capacity that has been added to or removed from the cell. The capacities are defined as:

$$Q_c(t) = \int_0^t I_c(t)dt \tag{1}$$

$$Q_d(t) = \int_0^t I_d(t)dt \tag{2}$$

In equations (1) and (2) I_c and I_d are charge and discharge currents and are assumed positive in value.

This approach is valid for analysing the discharge and charge RV characteristics independently. If the RVs are to be compared against a common capacity axis, instead of two separate capacity axes Q_c and Q_d, an initial condition must be introduced and the current I is assumed positive for discharge and negative for charge. The common capacity scale, known as the remaining capacity (Q_r), is now defined as:

$$Q_r(t) = Q_r(0) - \int_0^t I(t)dt \tag{3}$$

$$I(t) > 0 \quad \text{Discharge}$$

$$I(t) < 0 \quad \text{Charge}$$

Traditionally, when RV_c and RV_d curves are plotted against the common axis, Q_r, an erroneous hysteretic behaviour may be observed. The apparent hysteresis artefact arises due to the testing procedure and in the assumption that the remaining capacity is zero ($Q_r(0) = 0$) at the end of the discharge prior to the start of the RV_c test. For example the cell needs to be discharged prior to the RV_c characterisation test, for which a 1C constant current discharge can be performed up to the cell cut-off voltage V_{min}. The test is terminated and after a 4 hour rest the RV is measured as the starting value of the RV_c test and the remaining cell capacity (Q_r) is assumed zero. In comparison, during the RV_d test, diffusion limitations are reduced as the cell is discharged incrementally to V_{min}, and this allows for more capacity to be removed before the cell reaches V_{min}. Thus, there can be a difference in RV_c and RV_d, due to a miss-match of initial conditions.

Section 4.1 of this paper will demonstrate the variation of discharge capacity with different step sizes. The remaining cell capacity (Q_r) will then again be assumed zero (since the cell reached V_{min}) for the RV_d test, however, the measured RV value after a 4 hour rest will be lower (due to more capacity removal) in comparison to the starting value of the RV_c test. Thus, when plotting RV_c and RV_d against remaining capacity an offset between the curves will be observed and invalidating any true hysteresis assessment. An example of this effect will be shown further in Section 4.2.1.

This offset between RV_c and RV_d can be eliminated by ensuring that the RV_c test characterisation is performed directly after a RV_d characterisation. By doing so, the state of

the cell for the start of the RV_c procedure will be the same from when the RV_d ended; eliminating any apparent offset and allowing the true hysteretic magnitude to be assessed. This approach will be implemented as the new test methodology, further described in section 3. Furthermore, as the cell is first incrementally discharged and then incrementally charged, the RVs for hysteresis assessment can be plotted against the extracted capacity Q_e which is defined as:

$$Q_e(t) = Q_e(0) + \int_0^t I(t)dt \tag{4}$$

$$I(t) > 0 \quad \text{Discharge}$$

$$I(t) < 0 \quad \text{Charge}$$

The advantage of using Q_e over Q_r for the hysteresis assessment plot is that the initial extracted capacity $Q_e(0)$ can be assumed zero when the cell is fully charged; while the initial remaining capacity value $Q_r(0)$ might not be known priori for a fully charged cell. However, the total capacity extracted during the incremental discharge procedure ($Q_{e,max}$) can be used as the cell capacity in subsequent analysis. Note that dividing equations (3) by $Q_{e,max}$ gives the corresponding SoC $z(t)$ of the cell.

$$z(t) = \frac{Q_r(0)}{Q_{e,max}} - \frac{1}{Q_{e,max}} \int_0^t I(t)dt \tag{5}$$

$$I(t) > 0 \quad \text{Discharge}$$

$$I(t) < 0 \quad \text{Charge}$$

2.3. Hysteresis modelled as a dynamic system

As shown in Figure 1, an ECM consists of an ideal voltage source (the OCV) that is a function of SoC. A monotonic static function or a piecewise linear interpolation function, relating the rest voltage to the cell SoC can be used if the empirically determined charge and discharge rest voltages yield negligible hysteresis (in the order of a few millivolts, as many commercially available cell cyclers record to the nearest millivolt).

In the presence of hysteresis, a single static function will not suffice. A model capable of transitioning between the charge and discharge rest voltage curve is required. The hysteresis

model presented here is the one proposed by G.L. Plett [38] and a re-derivation of the model is given below. In this model a hysteresis state variable h is added or subtracted from the average of the charge and discharge rest voltages (let the average rest voltage be $\overline{\mathrm{RV}}$).

$$\mathrm{RV(z)} = \overline{\mathrm{RV}}(z) + h(\mathrm{z}) \tag{6}$$

The hysteresis state variable h is obtained as a solution to the differential equation given in equation (7).

$$\frac{dh}{dz} = K(H(z) - h(z)) \tag{7}$$

Here, $H(z)$ is the difference between the charge or discharge rest voltage and the mean rest voltage, $H = \mathrm{RV_c} - \overline{\mathrm{RV}}$ or $H = \overline{\mathrm{RV}} - \mathrm{RV_d}$ and is positive when charging and negative when discharging. In equation (7) K determines the rate at which the hysteresis state $h(z)$ reaches $H(z)$. To simulate the ECM the hysteresis state variable should however be solved as a function of time, as such the left and right side of equation (7) is multiplied by $dz/dt = I/Q_n$. To ensure stability of the resulting Ordinary Differential Equation (ODE) the coefficient of h should remain negative and therefore the modulus of I/Q_n is used, resulting in the following expression:

$$\frac{dh}{dt} = K\left|\frac{I}{Q_n}\right|(H(z) - h(t)) \tag{8}$$

Finally for simulation purposes the first order ODE in equation (8) can be written in a standard discrete time (denoted by subscript i) form as follows:

$$h_{i+1} = h_i e^{\left(-K\left|\frac{I_i}{Q_n}\right|\Delta t\right)} + \left(1 - e^{\left(-K\left|\frac{I_i}{Q_n}\right|\Delta t\right)}\right)H(z_i) \quad i = 0, 1, \ldots \tag{9}$$

To simulate equation (9) the initial hysteretic state h_0, $H(z_i)$ as a function of SoC and the transition rate K are required. The initial condition h_0 can be set to zero when the charge/discharge history of the cell is unknown and $H(z_i)$ can be determined empirically. To determine and validate the transition rate K, RV values occurring in-between the charge and discharge RV characteristic curves are required.

The following sections detail the experimental procedures to evaluate the influence of discharge/charge step size on $\mathrm{RV_c}$ and $\mathrm{RV_d}$ characteristics and the characterisation of the hysteresis function $H(z_i)$ required for hysteresis modelling.

3. Experimental details

3.1. Cell Details

Experimental studies were performed on four different commercially available lithium-ion cells. The chemistry, rated capacity and format of each cell included in this study are listed in Table 1. These cells were unused, having spent ~1 year of storage at 10 ± 3 °C after delivery.

Cell	Chemistry	Rated Capacity (Ah)	Nominal Voltage (V)	Maximum C rate (10 Sec)	Format	Number of cells tested
1	NMC	40	3.7	8C	Pouch	5
2	LFP	20	3.2	15C	Pouch	6
3	NMC	2.2	3.6	2C	Cylindrical	8
4	NMC (LTO anode)	13.4	2.6	15C	Pouch	8

Table 1 Cell details

3.2. Discharge & charge rest voltage against step size test procedure

Rest voltage tests were conducted inside a temperature controlled chamber set at 25 °C and the charging and discharging of the cells was done via a commercial battery cycler. For the discharge rest voltage test (RV_d) the cells were initially fully charged via a constant current constant voltage (CC-CV) procedure using a 1C current and C/20 cut-off current. After the full charge, cells were allowed to rest for 4 hours and the initial RV_d measurement was recorded. The cells were then gradually discharged in 4 % of rated capacity steps using a 1C discharge current until the lower cut-off voltage was reached. After every discharge step, a 4 hour rest period was applied for cell relaxation and the rest voltage was recorded. The smaller the step size the higher the number of RV_d points (higher resolution) can be obtained; however, the longer the test period. The 4 % step size was selected as a trade-off between test duration and resolution of RV curve. Following a similar procedure the RV_d tests were also repeated in steps of 10 %, 25 %, 50 % and 100 % of rated capacity to study capacity variation with step size and validate the one-to-one relationship between OCV and discharge capacity as explained in Section 2.2.

For the charge rest voltage (RV_c) characterisation, the cells were discharged with a 1C constant current until the cells reached the cut-off voltage. The initial RV_c value was recorded after a 4 hour rest period and the cells were then gradually charged in steps of 4 % of the rated capacity using a 1C current; a 4 hour rest period was again applied after each step and the rest voltage was recorded at the end of rest period. As lithium-ion cells are normally charged using a CC-CV procedure, when the cells reached V_{max} the voltage is held until the current drops below C/20. The RV_C characterization test was also repeated for steps of 10 %, 25 % and 100 % of rated capacity following a similar procedure.

3.3. Proposed Rest Voltage Hysteresis Test Procedure

The proposed test procedure to characterise the level of hysteresis, starts by fully charging the cells using CC-CV method. The cells are then discharged in steps of 4 % of the rated capacity with a 1C current and a 4 hour rest after each step discharge until the cut-off voltage V_{min} is reached as explained in section 3.2. The cells are then charged in steps of 4 % with a 1C current and 4 hour rest period after each charge step. When the cell reaches its maximum cut-off V_{max} the cell is held in CV mode until the current reduces to less than C/20, and the test procedure ends.

4. Results and Discussion

4.1. Rest voltage characteristics when discharging and charging

The discharge rest voltage (RV_d) plotted against the discharge capacity Q_d for Cell 1 is shown in Figure 2(a). All the discharge rest voltages recorded by different step tests are consistent at a particular discharge capacity, Q_d point e.g. 20 Ah / 50 % SoC; the length of the rest period is however important for this conclusion. A shorter rest interval would not have allowed the battery to reach equilibrium and the recorded RV at a particular discharge capacity can deviate. Similar results were also obtained from the other three cells, as shown in Figure 2 (b), Figure 2(c) and Figure 2(d), indicating the effect of step size on the RV_d is negligible provided the rest time is sufficient (~4 hours) for cell equilibration.

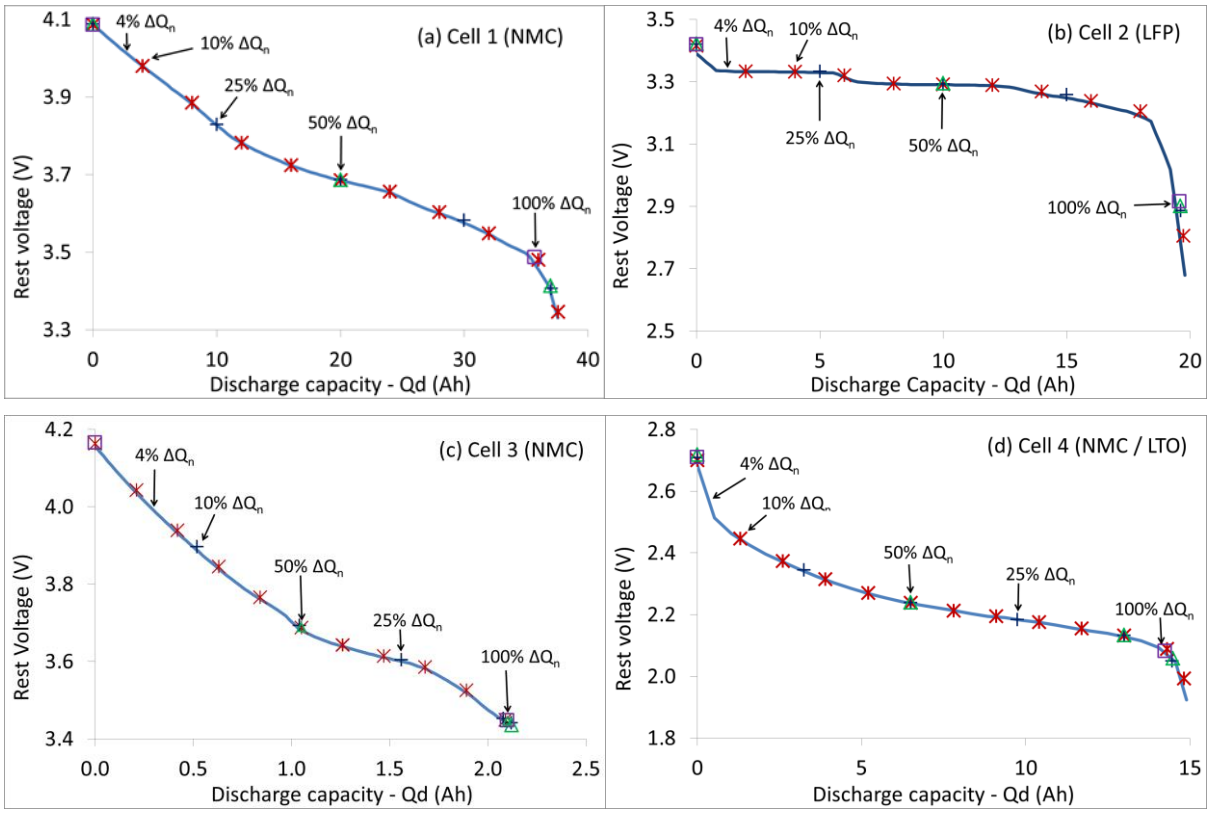

Figure 2: Rest voltage as a function of discharge capacity and varying step sizes for (a) 40 Ah NMC cell, (b) 20 Ah LFP cell, (c) 2.2 Ah NMC cell and (d) 13.4 Ah LTO cell.

From the RV test results, an increase in total discharge capacity with the decrease in discharge step size was observed. The variation of capacity with step size for all 4 types of cells is shown inTable 2. The capacities shown are the average over the number of cells and the error values show the 95 % confidence intervals which include cell to cell variation and

measurement error. From Table 2, it can be seen that there is capacity reduction of 5.0 % for Cell 1 and 4.1 % for Cell 4 when the cells are discharged continuously (100 % step size) in contrast to a 4 % step discharge (1C): in contrast the capacity variation of Cell 2 and Cell 3 is within the standard error. Note that the current used to discharge a cell is however the same (1C) for all step sizes. This has not been acknowledged in previously published research.

As a cell approaches complete discharge, a reduction in total discharge capacity with increase in step size can be expected. A larger step size relates to a larger discharge time period which corresponds to higher polarisation effects within a cell [35]. As such the cell terminal voltage can drop rapidly to its cut-off voltage V_{min} ending the test. With a smaller step size polarisation time is reduced and will in general allow more capacity to be discharged before the cell reaches its cut-off voltage.

The reduction in discharge capacity of Cells 2 and 3 with the 100 % step size is small in comparison to Cells 1 and 4. This suggests that the active material particles are almost fully lithiated when discharged continuously and discharging in 4 % steps only leads to a minor increase in total discharge capacity due to the reduced polarisation time effect. Factors that affect the lithiation process of electrode active material include porosity, tortuosity, particle size and solid phase diffusion coefficient can affect the lithiation process of the active material [42, 43] . As such the percentage capacity increase via incremental discharge can vary for different cells due to variations in manufacturing processes.

Step Size	Total discharge capacity $Q_{e,max}$ (Ah)			
	Cell 1	Cell 2	Cell 3	Cell 4
100 %	35.86 ± 0.09	19.17 ± 0.08	2.09 ± 0.01	14.36 ± 0.03
50 %	37.11 ± 0.07	19.19 ± 0.07	2.10 ± 0.01	14.59 ± 0.03
25 %	37.14 ± 0.07	19.19 ± 0.08	2.11 ± 0.01	14.57 ± 0.03
10 %	37.67 ± 0.03	19.26 ± 0.07	2.09 ± 0.01	14.89 ± 0.02
4 %	37.66 ± 0.04	19.31 ± 0.09	2.11 ± 0.01	14.95 ± 0.01
Maximum percentage capacity decrease	5.0 %	0.7 %	0.1 %	4.1 %

Table 2: Total discharge capacity $\boldsymbol{Q_{e,max}}$ with respect to discharge step size

Figure 3 shows the charge rest voltage (RV_c) against charge capacity Q_c for all the cells. Similar to the RV_d characteristic, RV_c recorded by different step sizes are consistent at a particular charge capacity Q_c point. The effect of step size on RV_c is therefore negligible provided sufficient rest time (~4 hours) is allowed between charge increments for cell equilibration.

However, in contrast to the RV_d tests the total charge capacities were similar for all step sizes. This outcome can be expected due to the testing procedure, as in the RV_c test, the charging current is allowed to drop when the cell voltage reaches V_{max} (constant voltage (CV) charging) and charging is stopped when the current drops to or below C/20. Therefore, this procedure charges the cells to a similar total capacity regardless of the step size, since the CV charging dominates the end of the charge for all step size.

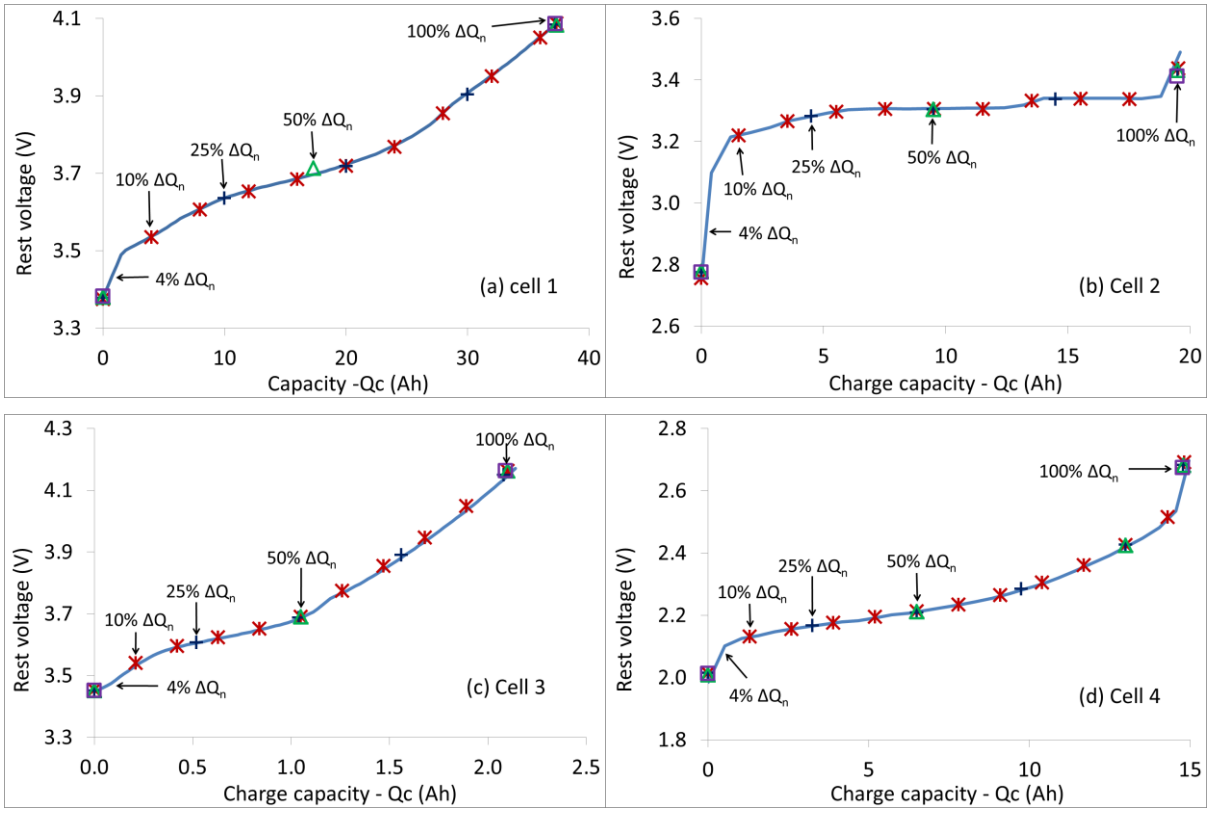

Figure 3: Rest voltage as a function of charge capacity and varying step sizes for (a) 40 Ah NMC cell, (b) 20 Ah LFP cell, (c) 2.2 Ah NMC cell and (d) 13.4 Ah LTO cell.

4.2. Hysteresis assessment of cells

4.2.1. Apparent increase in hysteresis

In section 2.2 the possible occurrence of an erroneous hysteretic behaviour was explained; Figure 4 demonstrates such an example and many others can be found in literature [32, 35]. In the figure, the rest voltages RV_c and RV_d of Cell 1 (NMC) are plotted against the remaining capacity Q_r as in the standard methods. Note that a 1C continuous discharge was performed to arrive at the 0 % point on the RV_c curve while a 4 % incremental discharge with rest was performed to arrive at the 0 % point on the RV_d curve. The extra gain in capacity from the incremental discharge procedure implies that the remaining capacity ($Q_r(0)$ in equation 3) will be different from the continuous discharge. However, if this initial remaining capacity is assumed zero as is often assumed in the literature, since the cell reached V_{min}, an incorrect offset between the RV_c and RV_d characteristic curves is introduced. Figure 4 therefore incorrectly indicates the existence of hysteresis across the full remaining capacity range.

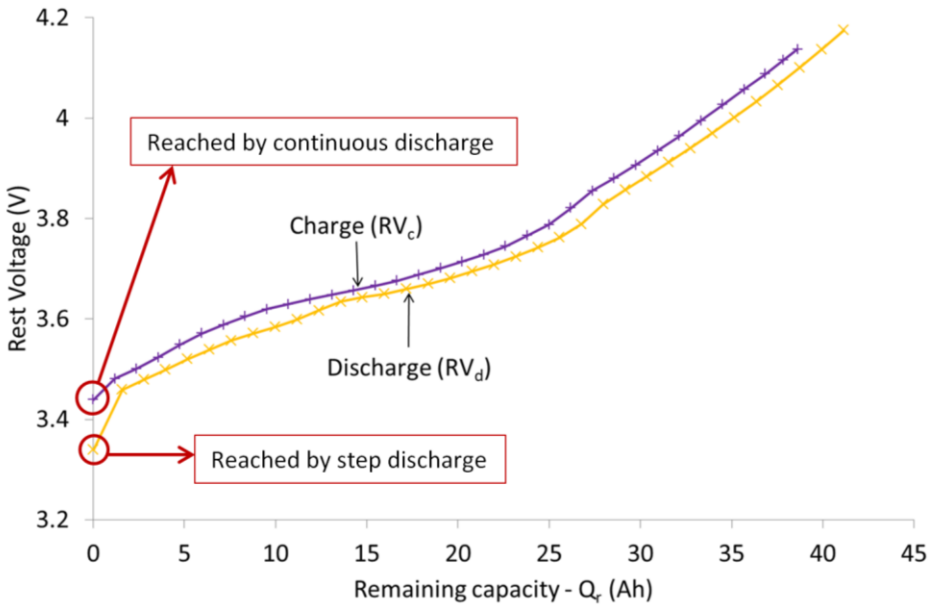

Figure 4: Plot of RV_c and RV_d with a misleading assessment of hysteresis when the initial remaining capacity is incorrectly assumed to be zero for 40 Ah NMC cell (cell 1).

4.2.2. Rest voltage and hysteresis against SoC

Following the hysteresis characterisation procedure described in Section 3.3, Figure 5 demonstrates the RV_c and RV_d curves from the same cell plotted against the extracted

capacity Q_e. This approach, as explained in Section 2.2, leads to a more accurate assessment of the level of hysteresis within the cell.

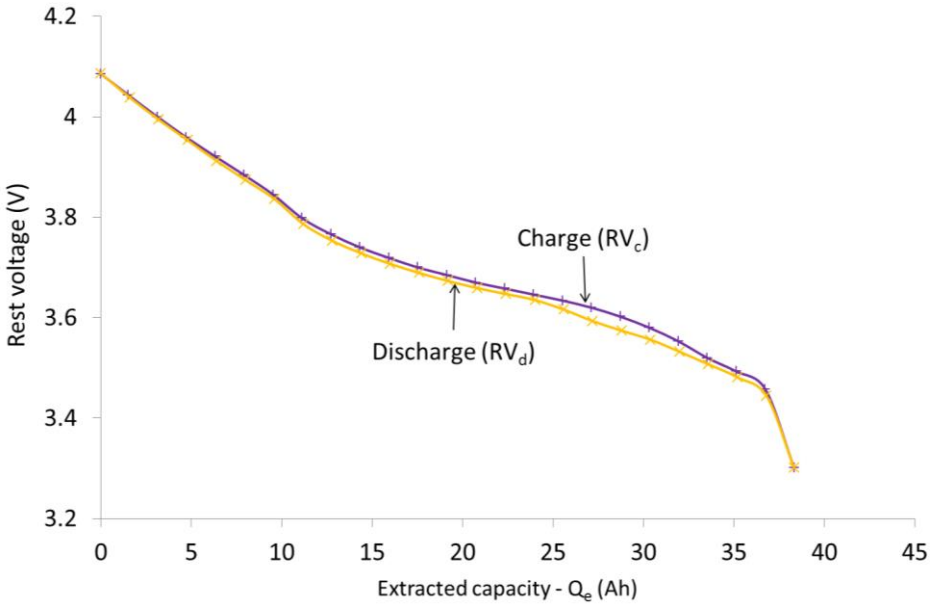

Figure 5: Rest voltage as a function of charge and discharge capacity with 4 % ΔQ_n step sizes when initial condition was matched for 40Ah NMC cell (Cell 1).

In comparison to Figure 4, Figure 5 indicates that the level of hysteresis is not significant across the full extracted capacity range. Furthermore, from the test procedure an estimate of $Q_{e,max} = 38$Ah for the cell maximum extracted capacity is obtained. This value can be used to calculate the SoC via equation (3) with $Q_r(0)$ set to 38Ah.

The charge and discharge RV curves against SoC for Cell 1 allow the calculation of hysteresis voltage which is shown as a function of SOC in Figure 6 (a). Though the cell is discharged in uniform steps, the last RV_d data point is decided when the cell reaches V_{min} for which the extracted capacity can be less than the step size. Similarly, during charge the capacity added when determining the last RV_c data point can be different from the predefined step size. The measured RV_d and RV_c data points will therefore not be determined at the same SoC. As such, the RV_c and RV_d curves are linearly interpolated to a reference SoC spanning from 0 to 100 % in increments of 1 % SoC in order to calculate the hysteresis voltage as shown in Figure 6.

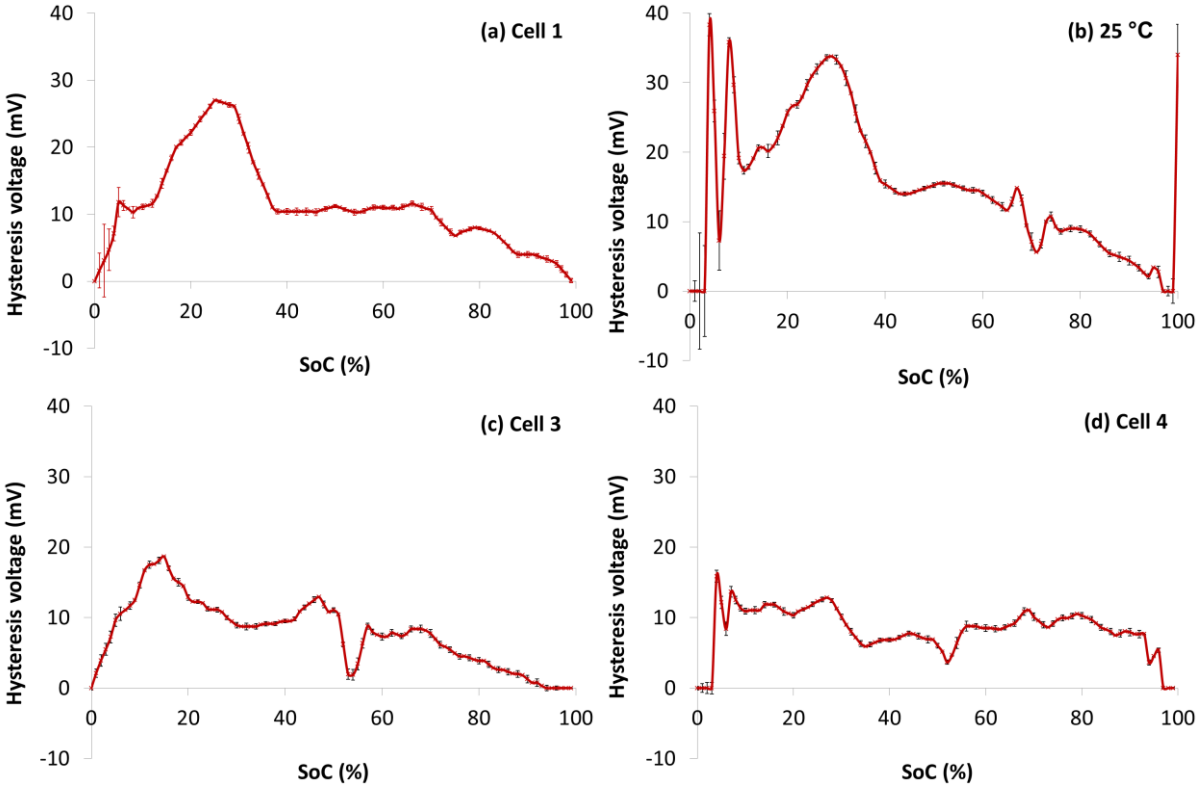

Figure 6: Hysteresis voltage vs SoC for (a) 40 Ah NMC cell, (b) 20 Ah LFP cell, (c) 2.2 Ah NMC cell and (d) 13.4 Ah LTO cell. Error bars shows standard error among cells tested.

Referring to Figure 6 (a), a hysteresis voltage of at least 10mV is present from 5 % to 70 % SoC and peaks to a maximum of 27mV at 25 % SoC. A similar hysteresis voltage was obtained for all the remaining cells of Cell 1 (NMC pouch).

Figure 6 (b) to (d) display the hysteresis voltages for Cell 2 (LFP pouch), Cell 3 (NMC cylindrical) and Cell 4 (LTO pouch) respectively. Cell 2 showed the highest level of hysteresis which was 38 mV near 5 % SoC and Cell 4 had the least level of hysteresis with a maximum of 16 mV near 5 % SoC. In general, maximum hysteresis was found within the 5 % to 25 % SoC range of all the cells tested.

The hysteresis voltage of LFP cell presented in Figure 6 (b), is considerably lower than the hysteresis of LFP cell reported previously [32, 33, 35]. The hysteresis voltage of other cell types shown in Figure 6 is shown for first time here. The results indicate that RV hysteresis assessment should not only be restricted to Li-ion LFP chemistry active material batteries, but also applied to NMC and LTO batteries as well if an accurate OCV is important; e.g. subsequent use in a battery model.

4.3. Rest voltage hysteresis and model simulation

A dynamic model for hysteresis was presented in the Open Circuit Voltage Section 2.3 and an empirically determined hysteresis voltage as a function of SoC was presented in the preceding section. The model (equation 9) can now be simulated to evaluate the rest-voltage transition at intermediate SoCs. Cell 1 and its hysteresis voltage (Figure 6) are used as an example in the following section to illustrate the simulation.

To assess the hysteresis transition a scenario is considered where the initial SoC is assumed to be at 30 % and then the battery is fully charged to 100 %, discharged to 10 % and charged back to 30 %. This scenario was selected to represent a typical EV usage window i.e. overnight charging, daily usage including recharge before travelling to base/home. In the absence of prior knowledge of a cell's charge/discharge history the initial hysteresis state is assumed zero ($h_0 = 0$) and the RV for the initial SoC is the average value of RV_c and RV_d. Two cases are considered with regards to the hysteresis voltage $H(z_i)$. In case 1, as often assumed in literature [38, 44], $H(z)$ is set to a constant and set equal to half the maximum hysteresis voltage, which for Cell 1 is $H(z) = 13.5$mV, and in case 2, it is assumed to be a function of the SoC and is set equal to half the empirically determined hysteresis voltage (shown in Figure 6). As stated in Section 2.3, to set the transition rate K of equation 9, RV data points occurring in between the RV_c and RV_d curves are required. In the absence of intermediate RV data the rate can be set arbitrarily and in the simulation the value is set at $K = 50$.

Figure 7 (a) and (b) demonstrate the outcome of the two cases. Setting the hysteresis voltage to a constant, the model overshoots both charge and discharge RV, whereas when the hysteresis voltage is assumed to be a function of the SoC the model follows the empirically determined RV_c and RV_d characteristics.
Figure **8** shows the corresponding error between the model and the RV_c and RV_d curves as a function of time for the two cases. For Case 1, the error starts at 12mV but rapidly decreases and overshoots to an error magnitude of around 10mV and higher deviations (approximately 25mV) are observed when the current changes direction causing the model to transit to the discharge curve. For Case 2, the RV error again starts at 12mV and rapidly falls close to zero as the model transits towards the RV_c curve and remains close to zero. The error deviates when the current changes direction causing the model to transit on to the RV_d curve. This

demonstrates that although Plett's model provides a method to include hysteresis, significant improvements in model predictions can be realised through adoption of the proper characterisation methods.

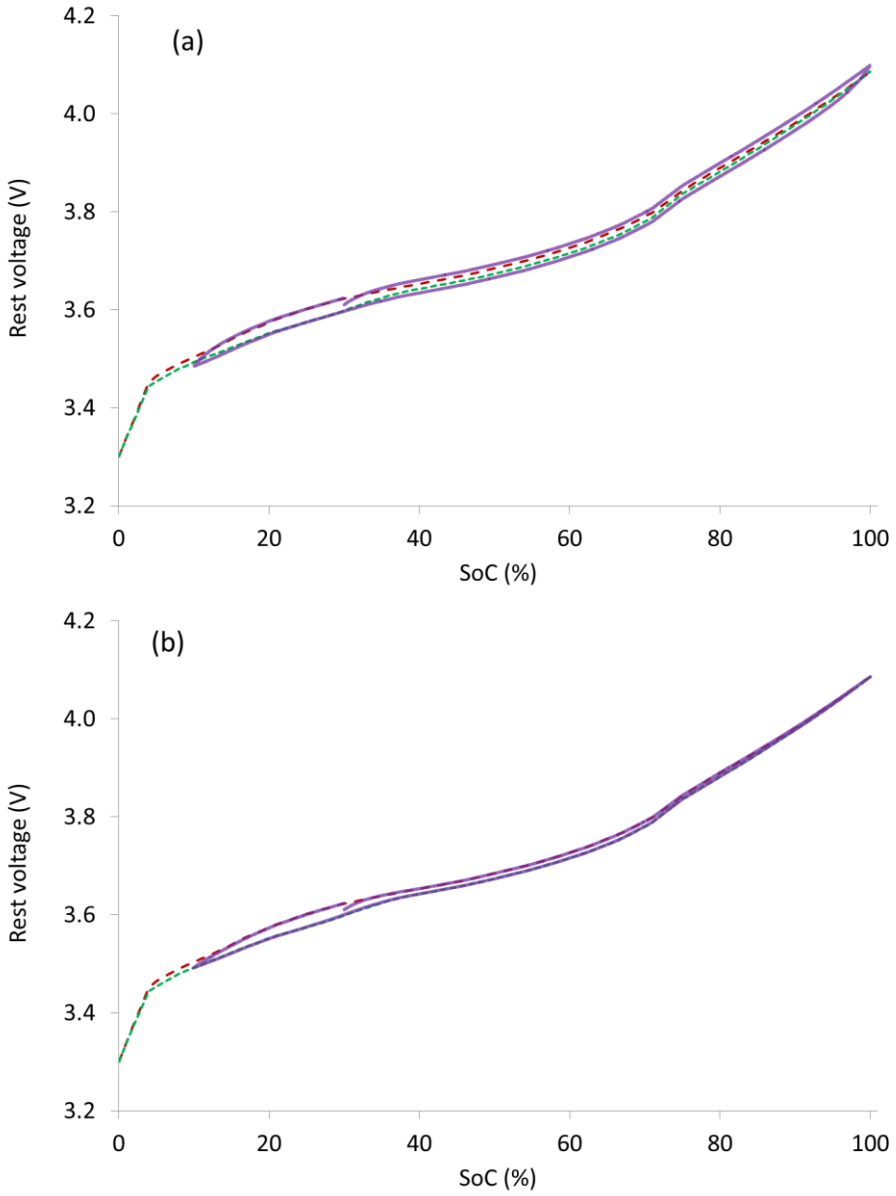

Figure 7: Hysteresis model transition with (a) the hysteresis voltage (solid purple) assumed a constant $\boldsymbol{H}(\boldsymbol{z}) = \boldsymbol{H}_{\boldsymbol{max}}$, (b) the hysteresis voltage $\boldsymbol{H}(\boldsymbol{z})$ (solid purple) assumed to be a function of SoC. The transition model in (a) can deviate from the RV_c (long red dash) and RV_d (short green dash) characteristic curves, (b) follows the RV_c and RV_d more closely.

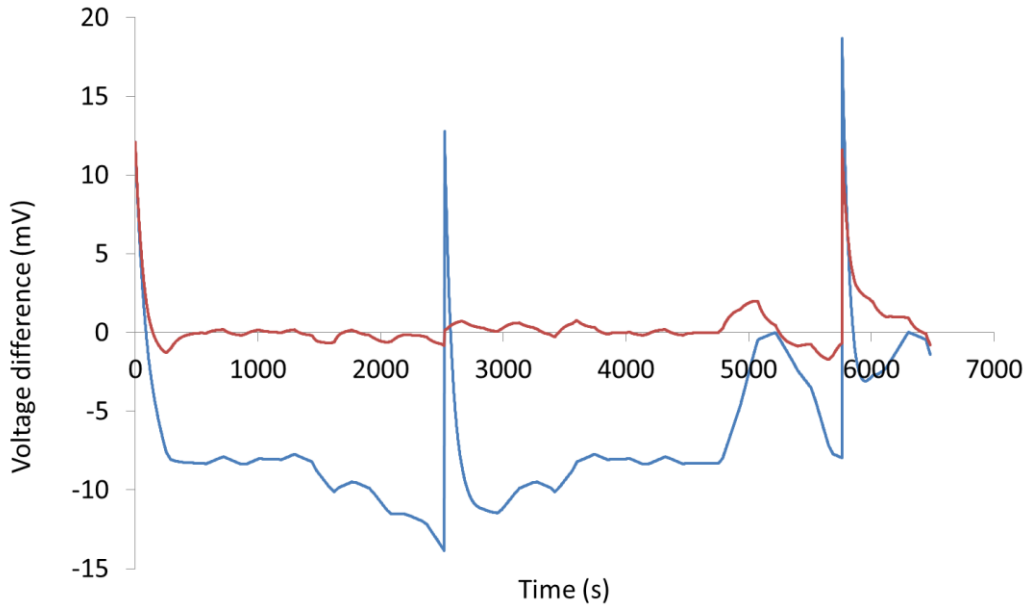

Figure 8: Voltage difference between transitioning rest voltage and RV_c and RV_d curves. Blue line: Case 1, constant hysteresis simulations; Red line: Case 2, adaptive hysteresis.

Work by earlier authors [38, 44] have assumed a constant hysteresis voltage and usually only for LFP batteries. In contrast the empirically determined rest voltages and hysteresis transition model presented here highlight that hysteresis assessment is not only restricted to LFP. In addition to assume a constant hysteresis voltage over the full SoC will contribute towards an error when simulating the battery voltage. Therefore, the hysteresis voltage should be characterised as a function of SoC when modelling the OCV element of an ECM incorporated as part of BMS.

5. Conclusions

Existing OCV and OCV hysteresis test methodologies fail to provide an accurate measure of OCV, which leads to inconsistent assessment of hysteresis. Multiple reasons have been identified as the root cause, i.e. inadequate use of rest period, capacity variation with test procedure, offset of RV_c and RV_d plots. In this work a new test methodology has been proposed which will address the root causes and accurately assess RV_c and RV_d, and subsequently, hysteresis.

Via the proposed methodology, the OCV and level of hysteresis of four li-ion battery types have been studied. The total discharge capacity in general increases with the decrease in

discharge step size (i.e. increase of number of step). The main cause of this capacity variation has been identified as the reduced polarization due to the additional rest steps in-between of the discharge phase of the test. The effect of step size on the measured RV_c and RV_d plots is negligible, provided they are plotted versus capacity, rather than SoC.

In hysteresis assessment, not only LFP cells but also NMC and LTO cells have exhibited hysteresis. The LFP cell (Cell 2) showed the highest level of hysteresis and the NCM cell with LTO anode (Cell 4) had the least level of hysteresis. In general, maximum hysteresis was present close to end of discharge (low SoC) for all the cells tested. The interaction of many particles with non-monotonic chemical potentials explains how hysteresis can occur in other Li-ion chemistries in addition to LFP.

From the results obtained a dynamic hysteresis model has been evaluated to provide an example of the enhancement can be achieved using the results generated following the methodology proposed in this paper. The inclusion of the hysteresis voltage as a function of SoC, rather than a constant, shows how the model predicts the empirically determined RV_c and RV_d characteristics more accurately.

The results reported in this paper demonstrate that careful consideration of the experimental methods, such as the charge/discharge procedure of a battery, is required to measure the OCV characteristics and allow subsequent assessment of hysteresis. The corresponding OCV characterisation procedure developed here will lead to consistent OCV curves within an acceptable experimental time and effort. Therefore, this methodology will be a useful guideline for both industrial and academic battery OCV and hysteresis assessment.

Acknowledgement

The research presented within this paper is supported by the Innovate UK through the WMG Centre High Value Manufacturing (HVM) Catapult in collaboration with Jaguar Land Rover and TATA Motors. The authors are thankful to Dr. Gael H. Chouchelamane and Dr. Chris Lyness from Jaguar Land Rover, Mr John Palmer and Dr. Yue Guo from WMG, and all 'cell work-stream' members of HVM Catapult for their valuable advice, comments and discussions.

Reference

[1] Y. Nishi, Journal of Power Sources, 100 (2001) 101-106.
[2] S.M. Lukic, J. Cao, R.C. Bansal, F. Rodriguez, A. Emadi, Industrial Electronics, IEEE Transactions on, 55 (2008) 2258-2267.
[3] B. Scrosati, J. Garche, Journal of Power Sources, 195 (2010) 2419-2430.
[4] S. Bourlot, P. Blanchard, S. Robert, Journal of Power Sources, 196 (2011) 6841-6846.
[5] J. Gomez, R. Nelson, E.E. Kalu, M.H. Weatherspoon, J.P. Zheng, Journal of Power Sources, 196 (2011) 4826-4831.
[6] S. Rodrigues, N. Munichandraiah, A.K. Shukla, J Solid State Electrochem, 3 (1999) 397-405.
[7] V. Sauvant-Moynot, J. Bernard, R. Mingant, A. Delaille, F. Mattera, S. Mailley, J.-L. Hognon, F. Huet, Oil Gas Sci. Technol. – Rev. IFP, 65 (2010) 79-89.
[8] M. Ecker, J.B. Gerschler, J. Vogel, S. Käbitz, F. Hust, P. Dechent, D.U. Sauer, Journal of Power Sources, 215 (2012) 248-257.
[9] J. Wang, P. Liu, J. Hicks-Garner, E. Sherman, S. Soukiazian, M. Verbrugge, H. Tataria, J. Musser, P. Finamore, Journal of Power Sources, 196 (2011) 3942-3948.
[10] W. Waag, S. Käbitz, D.U. Sauer, Applied Energy, 102 (2013) 885-897.
[11] H.L. Chan, S. D., in: Power Engineering Society Winter Meeting, 2000. IEEE, 2000, pp. 470-475 vol.471.
[12] D. Andre, M. Meiler, K. Steiner, H. Walz, T. Soczka-Guth, D.U. Sauer, Journal of Power Sources, 196 (2011) 5349-5356.
[13] T. Osaka, T. Momma, D. Mukoyama, H. Nara, Journal of Power Sources, 205 (2012) 483-486.
[14] M.D. Levi, G. Salitra, B. Markovsky, H. Teller, D. Aurbach, U. Heider, L. Heider, Journal of The Electrochemical Society, 146 (1999) 1279-1289.
[15] H.-M. Cho, Y.J. Park, H.-C. Shin, Journal of The Electrochemical Society, 157 (2010) A8-A18.
[16] J.P. Schmidt, T. Chrobak, M. Ender, J. Illig, D. Klotz, E. Ivers-Tiffée, Journal of Power Sources, 196 (2011) 5342-5348.
[17] L. Liao, P. Zuo, Y. Ma, X. Chen, Y. An, Y. Gao, G. Yin, Electrochimica Acta, 60 (2012) 269-273.
[18] T. Momma, M. Matsunaga, D. Mukoyama, T. Osaka, Journal of Power Sources, 216 (2012) 304-307.

[19] D.P. Abraham, E.M. Reynolds, P.L. Schultz, A.N. Jansen, D.W. Dees, Journal of The Electrochemical Society, 153 (2006) A1610-A1616.
[20] T. Huria, G. Ludovici, G. Lutzemberger, Journal of Power Sources, 249 (2014) 92-102.
[21] C. Zhang, J. Jiang, W. Zhang, S.M. Sharkh, Energies, 5 (2012) 1098-1115.
[22] L. Lu, X. Han, J. Li, J. Hua, M. Ouyang, Journal of Power Sources, 226 (2013) 272-288.
[23] J. Warner, 7 - Lithium-Ion Battery Packs for EVs, in: G. Pistoia (Ed.) Lithium-Ion Batteries, Elsevier, Amsterdam, 2014, pp. 127-150.
[24] K.G. Gallagher, P.A. Nelson, 6 - Manufacturing Costs of Batteries for Electric Vehicles, in: G. Pistoia (Ed.) Lithium-Ion Batteries, Elsevier, Amsterdam, 2014, pp. 97-126.
[25] V. Srinivasan, J.W. Weidner, J. Newman, Journal of The Electrochemical Society, 148 (2001) A969-A980.
[26] V. Srinivasan, J. Newman, Electrochemical and Solid-State Letters, 9 (2006) A110-A114.
[27] U.S.D.o. Energy, in: V.T.P. Energy Efficiency and Renewable Energy (Ed.), Idaho Operations Office, 2010.
[28] I. 62660-1, in, International Electrotechnical Commission, Geneva, Switzerland, 2012.
[29] B.I. 12405-2:2012, in, British Standards Institution 2012.
[30] W. Dreyer, J. Jamnik, C. Guhlke, R. Huth, J. Moskon, M. Gaberscek, Nat Mater, 9 (2010) 448-453.
[31] M. Fleckenstein, O. Bohlen, M.A. Roscher, B. Bäker, Journal of Power Sources, 196 (2011) 4769-4778.
[32] M.A. Roscher, O. Bohlen, J. Vetter, International Journal of Electrochemistry, 2011 (2011).
[33] X. Tang, X. Mao, J. Lin, B. Koch, in: American Control Conference, San Francisco, CA, USA, 2011.
[34] K. Jonghoon, S. Gab-Su, C. Changyoon, C. Bo-Hyung, L. Seongjun, in: Electric Vehicle Conference (IEVC), 2012 IEEE International, 2012, pp. 1-5.
[35] M. Petzl, M.A. Danzer, Energy Conversion, IEEE Transactions on, 28 (2013) 675-681.
[36] P.A. Derosa, P.B. Balbuena, Journal of The Electrochemical Society, 146 (1999) 3630-3638.
[37] P. G. Bruce, A. Robert Armstrong, R. L. Gitzendanner, Journal of Materials Chemistry, 9 (1999) 193-198.
[38] G.L. Plett, Journal of Power Sources, 134 (2004) 262-276.
[39] B. Pattipati, B. Balasingam, G.V. Avvari, K.R. Pattipati, Y. Bar-Shalom, Journal of Power Sources, 269 (2014) 317-333.
[40] V. Pop, H.J. Bergveld, J.H.G. Op het Veld, P.P.L. Regtien, D. Danilov, P.H.L. Notten, Journal of The Electrochemical Society, 153 (2006) A2013-A2022.
[41] A. Barai, G.H. Chouchelamane, Y. Guo, A. McGordon, P. Jennings, Journal of Power Sources, 280 (2015) 74-80.
[42] K. Smith, C.-Y. Wang, Journal of Power Sources, 161 (2006) 628-639.
[43] I.V. Thorat, D.E. Stephenson, N.A. Zacharias, K. Zaghib, J.N. Harb, D.R. Wheeler, Journal of Power Sources, 188 (2009) 592-600.
[44] X. Hu, S. Li, H. Peng, Journal of Power Sources, 198 (2012) 359-367.